JACS
JOURNAL OF THE AMERICAN CHEMICAL SOCIETY
pubs.acs.org/JACS
Article

# High-Capacitance Pseudocapacitors from $Li^+$ Ion Intercalation in Nonporous, Electrically Conductive 2D Coordination Polymers

Harish Banda,[⊥] Jin-Hu Dou,[⊥] Tianyang Chen, Nicole J. Libretto, Madhusudan Chaudhary, Guy M. Bernard, Jeffrey T. Miller, Vladimir K. Michaelis, and Mircea Dincă*

Cite This: https://dx.doi.org/10.1021/jacs.0c10849 Read Online





**ABSTRACT:** Electrochemical capacitors (ECs) have emerged as reliable and fast-charging electrochemical energy storage devices that offer high power densities. Their use is still limited, nevertheless, by their relatively low energy density. Because high specific surface area and electrical conductivity are widely seen as key metrics for improving the energy density and overall performance of ECs, materials that have excellent electrical conductivities but are otherwise nonporous, such as coordination polymers (CPs), are often overlooked. Here, we report a new nonporous CP, $Ni_3$(benzenehexathiolate) ($Ni_3BHT$), which exhibits high electrical conductivity of over 500 S/m. When used as an electrode, $Ni_3BHT$ delivers excellent specific capacitances of 245 F/g and 426 F/$cm^3$ in nonaqueous electrolytes. Structural and electrochemical studies relate the favorable performance to pseudocapacitive intercalation of $Li^+$ ions between the 2D layers of $Ni_3BHT$, a charge-storage mechanism that has thus far been documented only in inorganic materials such as $TiO_2$, $Nb_2O_5$, and MXenes. This first demonstration of pseudocapacitive ion intercalation in nonporous CPs, a class of materials comprising thousands of members with distinct structures and compositions, provides important motivation for exploring this vast family of materials for nontraditional, high-energy pseudocapacitors.

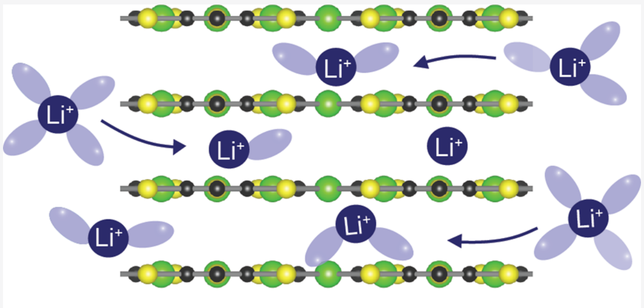


## INTRODUCTION

Electrochemical double layer capacitors (EDLCs) store energy through rapid and reversible electrolytic ion sorption on charged electrode surfaces.[1] The nonfaradaic nature of this physisorptive process allows for high deliverable power densities but also leads to relatively low energy density.[2,3] One strategy to enhance the energy density is to increase the specific surface area (SSA), and thus the area available for ion electrosorption, while maintaining high electrical conductivity. This is difficult: the only materials that exhibit both high conductivity and high surface area are various types of carbon, including graphene and its derivatives, or more recently certain coordination networks.[4−8] An alternative strategy to increase the energy density has been the use of pseudocapacitive electrode materials.[9,10] These materials often exhibit low SSAs but still deliver excellent charge storage capabilities through faradaic redox processes that are not limited by solid-state ion diffusion.[11−13] Originally demonstrated as a surface-based redox process in $RuO_2$ and $MnO_2$,[14,15] the pseudocapacitive mechanism has been also described as intercalation-based in transition metal oxides ($TiO_2$, $Nb_2O_5$)[16−18] and 2D layered materials ($Ti_3C_2$, $MoS_2$).[19−22] Despite their intrinsically nonporous nature, these materials deliver high energy and power densities through rapid pseudocapacitive intercalation of ions between the 2D layers or within the one-dimensional channels of their bulk lattices.[9] Nevertheless, this promising charge-storage mechanism has thus far been limited to a select few inorganic materials and warrants further development of new electrode materials that can build on recent progress.

One class of emerging materials that offer high electrical conductivities and layered structures with great compositional diversity and physicochemical properties are 2D CPs.[7,23,24] These materials accommodate $\pi$-conjugated organic ligands and transition metal ions in 2D nanosheets through extended $\pi$-d conjugation and are good candidates for ECs.[25−27] Indeed, porous CPs, commonly known as metal-organic frameworks (MOFs),[28] have already been explored as electrodes for EDLCs.[29,30] Among these, 2D materials that have high electrical conductivity and are porous have shown the greatest promise, although their operating voltage remains below 1 V in aqueous electrolytes.[31−34] Perhaps because of these recent

Received: October 13, 2020

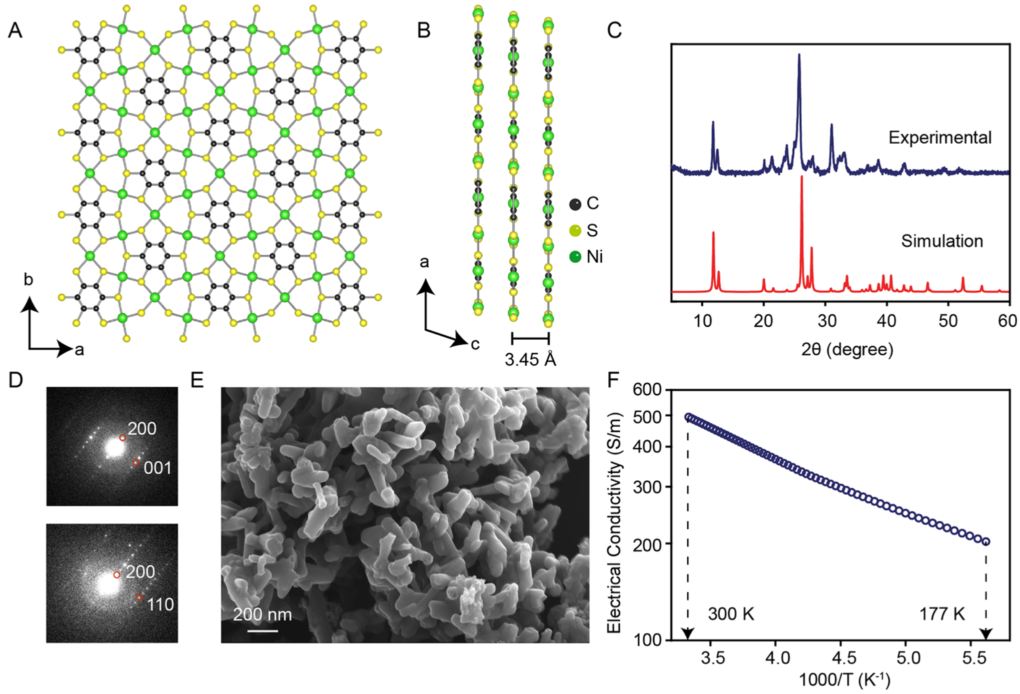


**Figure 1.** Simulated structure of $Ni_3BHT$ shown normal to the (A) *c* axis and (B) *b* axis. (C) X-ray diffraction patterns, (D) selected area diffraction patterns, and (E) scanning electron microscopy image of $Ni_3BHT$ powders. (F) Variable-temperature electrical conductivity of pressed $Ni_3BHT$ pellets obtained through the van der Pauw method.

advances with porous MOFs, related 2D CPs that are *nonporous* have received little attention in the context of energy storage, despite their excellent electrical properties.[24,27] Herein, we report that the new, nonporous CP $Ni_3BHT$ (BHT = benzenehexathiolate) is an excellent electrode material that stores charge through an intercalation-based pseudocapacitive mechanism. A high electrical conductivity of 500 S/m and a layered structure allow efficient intercalation of $Li^+$ ions in a nonaqueous $LiPF_6$/acetonitrile (MeCN) electrolyte to deliver a high gravimetric capacitance of 245 F/g. These results highlight the potential and benefits of designing and investigating nonporous layered materials in ECs.

## RESULTS

**Synthesis and Structural Characterization.** Microcrystalline samples of $Ni_3BHT$ were obtained through reaction of benzenehexathiol, $C_6S_6H_6$, with $NiCl_2{\cdot}6H_2O$ in deaerated methanol under anaerobic conditions for 24 h at room temperature (details in Supporting Information). Upon isolation from the mother liquor, $Ni_3BHT$ does not show weight loss below 200 °C and its electrical conductivity is maintained for at least 6 months in air (Figure S1). The powder X-ray diffraction (PXRD) pattern of as-synthesized $Ni_3BHT$ does not match that of the known phase $Ni_3BHT_2$ [27] and instead resembles that of $Cu_3BHT$ (Figure 1C).[24,35] Further analysis through selected area electron diffraction (SAED) revealed unit cell parameters $a = 14.16$ Å, $b = 8.86$ Å, $c = 3.45$ Å, $\alpha = 90°$, $\beta = 99.7°$, and $\gamma = 90°$ (Figure 1A,B,D and Figure S2) that indeed are similar to those of $Cu_3BHT$. Taken together, the PXRD and SAED data suggest that $Ni_3BHT$ is a new phase that bears close resemblance to $Cu_3BHT$, with 2D layers made up of square-planar $Ni^{2+}$ ions bonded to four S atoms in a square planar coordination and BHT ligands surrounded by six Ni atoms. These form a dense nonporous arrangement that contrasts with the structure of the known $Ni_3BHT_2$ that has a porous hexagonal honeycomb-type structure (Figure S3).[27] Elemental analysis found C and S content of 19.5% and 44.6%, respectively, close to the expected values for a chemical composition of $Ni_3C_6S_6$ for $Ni_3BHT$, and confirmed that the ligand does not suffer desulfurization during the reaction. Attempts to determine the Ni content through digestion methods have been hampered likely by the low solubility of NiS.

The bulk physical properties of $Ni_3BHT$ were studied using scanning electron microscopy (SEM), $N_2$ gas sorption analysis, and van der Pauw electrical conductivity measurements.[36] SEM images reveal rod-like structures that are larger than 100 nm in length and a few tens of nanometers in diameter (Figure 1E). $N_2$ sorption analysis determined a low Brunauer−Emmett−Teller (BET) SSA of ∼25 $m^2/g$ (Figure S4), in line with the expected nonporous nature of $Ni_3BHT$. Variable-temperature electrical conductivity of pressed $Ni_3BHT$ pellets demonstrated an excellent conductivity of ∼500 S/m at 298 K and a steady decline with decreasing temperature, as has been observed for several other bulk phases of 2D MOFs. Overall, the 2D layered structure of $Ni_3BHT$ and its high electrical conductivity and thermal stability encouraged us to evaluate its performance in ECs. Electrochemical analyses were performed using a 1 M lithium hexafluorophosphate ($LiPF_6$)/MeCN electrolyte, ensuring that the cation size is adequately small to potentially intercalate between $Ni_3BHT$ layers.

**Electrochemical Performance in ECs.** Cyclic voltammograms (CVs) of $Ni_3BHT$ powders pressed on Ni foam were obtainedin a three-electrode cell using sufficiently large porous carbon as a counter electrode and Ag wire as pseudoreference (details in Supporting Information). CVs obtained in increasingly large potential windows up to 1.7 V display distorted rectangular curves with no clear Faradaic peaks (Figure 2A). Stable, rectangular CVs are observed even when the scan rate is decreased to as low as 0.5 mV/s (Figure S5),


https://dx.doi.org/10.1021/jacs.0c10849
J. Am. Chem. Soc. XXXX, XXX, XXX−XXX

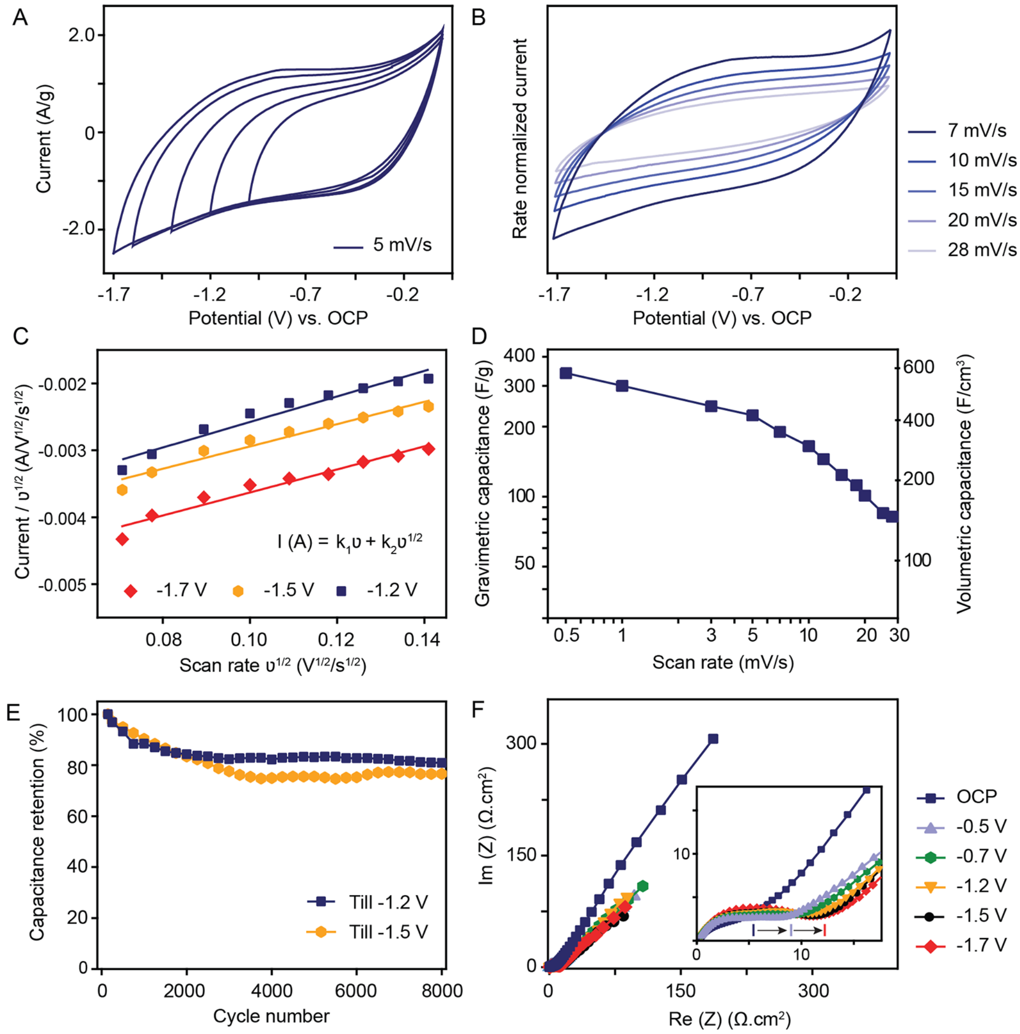


**Figure 2.** (A) Cyclic voltammetry (CV) curves of $Ni_3BHT$ in a three-electrode cell at a scan rate of 5 mV/s in increasing reductive potential windows from 1.0 to 1.7 V. (B) CVs in a range of scan rates from 7 to 28 mV/s in the largest tested potential window of 1.7 V. (C) Current vs scan rate analysis at select potentials of −1.2, −1.5, and −1.7 V vs open circuit potential (OCP). (D) Specific discharge capacitances obtained in a range of scan rates with corresponding time scales highlighted. (E) Capacitance retention under repeated cycling at a scan rate of 30 mV/s over 8000 cycles. (F) Imaginary versus real components of impedance (Nyquist plot) obtained at frequencies between 10 mHz and 200 kHz for $Ni_3BHT$ electrodes at OCP and various negative polarizations. Inset shows EIS responses at high frequencies, indicating a gradual increase in semicircle diameters with increasing polarization bias.

but scanning beyond −1.7 V vs open circuit potential (OCP) results in fast decay of current after multiple cycles (Figure S6). Altogether, the CV responses indicate reversible charge storage in $Ni_3BHT$ and also identify a stable working potential window of 1.7 V. Because the observed CVs are nearly rectangular, lack Faradaic features, and display nearly voltage-independent current in a given potential window, it is possible to derive true deliverable capacitances (in farads) instead of the overall charge stored (in coulombs or mAh).[37] Thus, $Ni_3BHT$ displays high specific capacitances of 245 F/g and 426 F/cm$^3$ at a scan rate of 3 mV/s, which are unusually high for materials with surface areas as low as that of $Ni_3BHT$. Indeed, in view of its low surface area, the large specific capacitance of $Ni_3BHT$ cannot be attributed to an ideal double-layer charge storage. An alternative mechanism is that of intercalation-based pseudocapacitance. Although pseudocapacitive behavior typically involves visible Faradaic features in the CVs, there are materials that operate through pseudocapacitance whose CVs are featureless, such as nonporous oxides $RuO_2$ and $Nb_2O_5$.[14,17] We note, however, that intercalation-based pseudocapacitance is rare: other than the oxides above, only MXenes, $TiO_2$, and $MoS_2$ are known to operate through this mechanism.

One means to interrogate the mechanism giving rise to the high capacitance of $Ni_3BHT$ is through electrochemical kinetic studies that assess the nature of ion sorption on the electrode. Dunn et al. have proposed a method to evaluate the capacitive contribution in a material by treating the total current as a sum of contributions from a diffusion-limited battery-type process that scales with the square root of the scan rate, $\upsilon^{1/2}$, and a surface-controlled capacitive (or pseudocapacitive) process that scales linearly with the scan rate.[9] The currents from the CVs in $Ni_3BHT$ were analyzed by plotting $i(V)/\upsilon^{1/2}$ vs $\upsilon^{1/2}$ for a range of scan rates at three different potentials of −1.2, −1.5, and −1.7 V vs OCP (Figure 2B,C). The slopes from these curves indicate that the majority of the current (~80%) originates from surface-controlled pseudocapacitive ion sorption whereas the rest (~20%) is from a diffusion-controlled battery-type process. Specific capacitances calculated from these curves reach high values of 195, 124, and 85


https://dx.doi.org/10.1021/jacs.0c10849
J. Am. Chem. Soc. XXXX, XXX, XXX−XXX

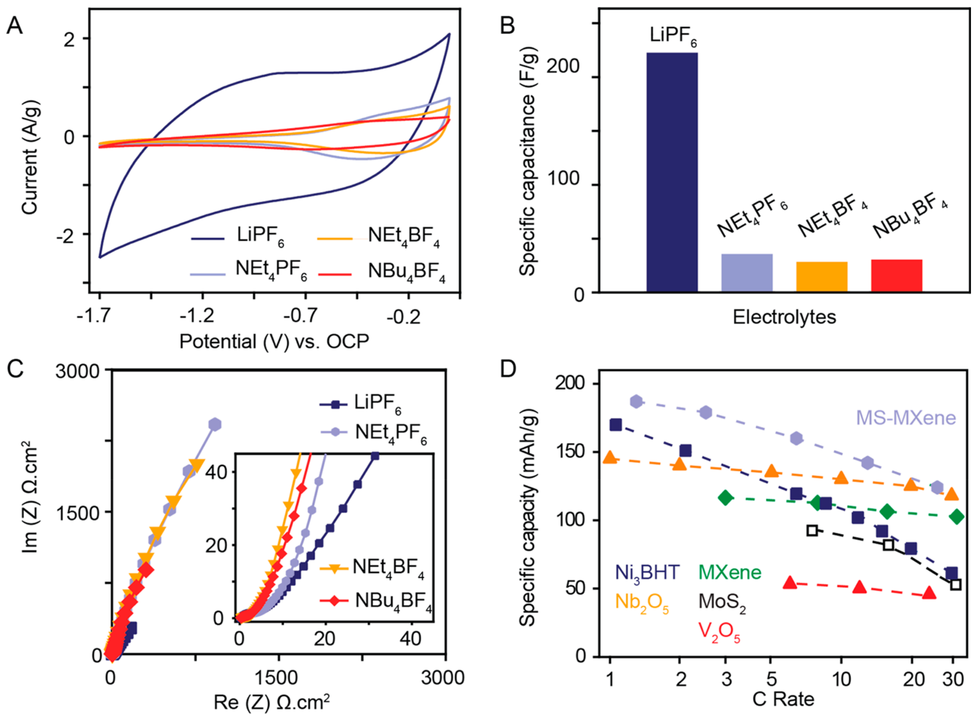


**Figure 3.** (A) CVs of $Ni_3BHT$ at a scan rate of 5 mV/s in 1 M $LiPF_6$, $NEt_4PF_6$, $NEt_4BF_4$, and $NBu_4BF_4$/MeCN electrolytes that have different electrolytic ion sizes. Electrolytes with large TAA cations display low and decreasing currents with stronger polarization. (B) Gravimetric capacitances and (C) Nyquist impedance spectra of $Ni_3BHT$ in the tested electrolytes. (D) Comparison of $Ni_3BHT$ with other pseudocapacitive materials reported in the literature. Materials with electrode mass loadings of ≥1.5 mg/cm$^2$ and potential windows of ≥1.5 V are compared (Supporting Table 2). MS-MXene indicates Mxene synthesized using molten salts at 750 °C.

F/g at scan rates of 7, 14, and 28 mV/s, respectively (Figure 2D). Long-term cycling studies of $Ni_3BHT$ at a fast scan rate of 30 mV/s (discharge in 56 s) in different potential windows indicate retention of over 80% after 8000 cycles (Figure 2E), although cycling in the widest window of 1.7 V decreases capacitance retention to 70% after 2000 cycles (Figure S7).

Electrochemical impedance spectra (EIS) were recorded at OCP under various negative polarizations to analyze the ion transport in $Ni_3BHT$ under dynamic conditions (Figure 2F). The EIS curves display extended 45° Warburg regions in the mid-frequency region and strong deviations from a vertical line in the lower frequency region, consistent with a nonideal capacitive behavior that is typically associated with limited ion transport in an electrode material.[38] In addition, a closer look at the high-frequency region finds an increase in the semicircle diameters with stronger polarizations (inset, Figure 2F), indicating that a charge transfer mechanism, typical of a pseudocapacitive electrode, is at play.[37] Warburg diffusion coefficients, $\sigma$, measured as the slope of real $Z$ vs $\omega^{-1/2}$, indicate values in the range of 6−9 $\Omega$ $S^{-1/2}$ cm$^2$ at various applied potentials (Figure S8). These values are on par with the value of 1.2 $\Omega$ $S^{-1/2}$ cm$^2$ reported for pseudocapacitive materials such as amorphous $TiO_2$.[39,40]

**Role of Electrolytic Ion Sizes.** With the evidence of pseudocapacitive behavior from CVs and EIS in hand, we sought to probe whether $Ni_3BHT$ displays the rare intercalation-based pseudocapacitance mechanism proposed thus far only for oxides and MXenes. To this end, we chose electrolyte salts with cations and anions of various sizes: tetraethylammonium hexafluorophosphate ($NEt_4PF_6$), tetraethylammonium tetrafluoroborate ($NEt_4BF_4$), and tetrabutylammonium tetrafluoroborate ($NBu_4BF_4$). A comparison of CVs obtained with these electrolytes demonstrates much lower current with tetraalkylammonium (TAA) cations relative to $Li^+$ (Figure 3A) and correspondingly lower capacitances of approximately 30 F/g compared to 227 F/g with $Li^+$ (Figure 3B). It should be noted here that the ionic conductivities for all the tested salts are similar (Supporting Table 1) and cannot be the origin for the observed differences. Changing the anion and comparing $NEt_4PF_6$ to $NEt_4BF_4$ leads to essentially identical CVs (Figure 3A), suggesting that any differences in behavior are caused by cations and that the ion sorption process is accordingly mainly cation-driven. CVs in TAA electrolytes further display nearly flat shapes with currents approaching zero at the terminal potentials when scanned cathodically from OCP. This behavior is reminiscent of size-based ion-sieving observed in porous carbons and pillared graphene. With these, ion sorption in macropores and onto the external surface of particles leads to notable currents in the first few hundred mV of polarization from OCP. The currents rapidly decrease to nearly zero at higher polarization due to restricted access into the micropores.[38,41−44] Because $Ni_3BHT$ is a nonporous material and lacks ultramicropores (<1 nm), the observed ion-sieving behavior could be attributed to its ordered 2D layered structure, wherein small $Li^+$ ions are able to intercalate but larger TAA ions are not. The latter ions only display minimal surface-based redox activity and ion sorption at polarizations close to OCP. Indeed, because $Li^+$ ions are small enough to intercalate, their response in the low frequency region of the EIS deviates significantly from the ideal vertical line and differs from that of the larger TAA ions, which are too bulky to intercalate (Figure 3C).

Overall, the electrochemical studies confirm that ion sorption in $Ni_3BHT$ is defined by cation size and that the


https://dx.doi.org/10.1021/jacs.0c10849
J. Am. Chem. Soc. XXXX, XXX, XXX−XXX

intercalation of ions into 2D layers drives the total capacitance. A comparison of $Ni_3BHT$ with other state-of-the-art pseudocapacitive electrodes in terms of specific capacity (mAh/g) at 1 C (Figure 3D and Supporting Table 2; 1 C = discharge in 1 h) reveals that the capacity of $Ni_3BHT$, 175 mAh/g, is surpassed only by MXenes, which exhibit 187 mAh/g at 1.3 C. It should be noted that whereas $Ni_3BHT$ is obtained via a room-temperature solution process, MXenes typically require molten salt synthesis at high temperature.[45] A steady decline in discharge capacities is also noted for $Ni_3BHT$ at high discharge rates of 10−30 C. This, together with the clear deviation from the ideal vertical line at low EIS frequencies expected for pseudocapacitive materials, points to impeded ion transport at high discharge rates. As with other materials operating through intercalation, optimizing crystallinity, particle size, current collector contacts, and material processing is likely to improve the power density of $Ni_3BHT$.

**Characterization of the Electrode Processes.** The structural and compositional evolution of $Ni_3BHT$ under potential bias was investigated using various *ex-situ* X-ray and solid-state nuclear magnetic resonance (SSNMR) spectroscopy techniques. PXRD patterns of a $Ni_3BHT$ electrode (details in Supporting Information) cycled and negatively polarized in 1 M $LiPF_6$/MeCN appear similar and suggest good retention of crystallinity, highlighting the stability of $Ni_3BHT$ under electrochemical conditions (Figure S9). Nevertheless, the absence of changes in the interlayer packing distance (*d* spacing) raises interesting aspects about intercalation in $Ni_3BHT$. Typically, intercalation in 2D materials can occur through two main pathways: (a) solvated electrolytic ions undergo partial or total desolvation in order to intercalate, resulting in minimal changes to the *d* spacing; (b) intercalation of the ions leads to significant exfoliation/layer separation within the electrode material. Although one may expect the latter to dominate in 2D materials due to weak van der Waals interlayer interactions, a recent study of MXenes using various Li-containing electrolytes found that the electrolytic $Li^+$ ions are able to undergo partial-to-full desolvation during intercalation. Depending on the nature of the solvent−electrode interactions, the intercalation does not always lead to changes in *d* spacing.[19] As suggested by the PXRD data and additional tests in various electrolytes (Supporting Note 1 and Figure S10), we believe that a similar desolvation−intercalation mechanism is at play in $Ni_3BHT$.

$^7$Li SSNMR spectra of $Ni_3BHT$ samples prepared either as soaked with electrolyte or as negatively polarized in ECs were compared to identify different chemical environments of $^7$Li during ion sorption under polarization. To provide a comparison point, similar tests were performed with $Ni_3HITP_2$ (HITP = 2,3,6,7,10,11-hexaiminotriphenylene), a related 2D *porous* CP (i.e., a MOF) that is known to adsorb ions in its micropores[34] and thereby provides a contrasting environment to the proposed pseudocapacitive intercalation in $Ni_3BHT$ (Supporting Note 2). $^7$Li NMR spectra for pristine $Ni_3BHT$ and $Ni_3HITP_2$ display strong isotropic peaks at approximately −3 and −1 ppm, respectively. We assign these peaks to $Li^+$ ions that are either associated with the outer surface of the particles ($Ni_3BHT$) or adsorbed in the $Ni_3HITP_2$ micropores. Upon polarization, $Ni_3BHT$ displays a clear shift in the peak position to ∼0 ppm, whereas that for $Ni_3HITP_2$ is unchanged. Furthermore, a closer examination of the spectrum for polarized $Ni_3BHT$ reveals an asymmetric peak, which manifests even more distinctly in its satellite peaks at approximately −70 and −73 ppm (inset, Figure 4A). The different chemical shifts in the polarized $Ni_3BHT$ sample

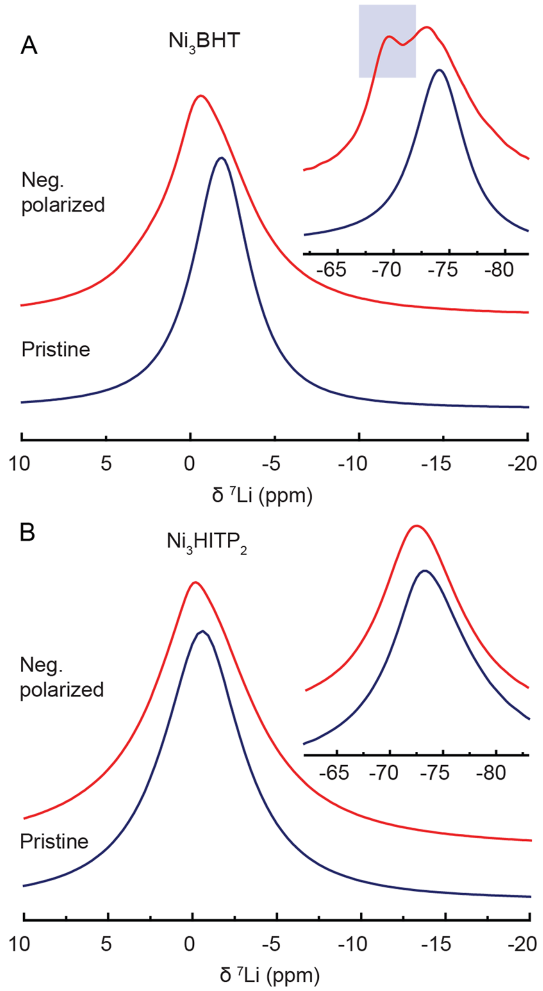


**Figure 4.** Comparison of $^7$Li NMR spectra of soaked and negatively polarized (A) $Ni_3BHT$ and (B) $Ni_3HITP_2$ in 1 M $LiPF_6$/MeCN. Insets show satellite peaks of $Ni_3BHT$ and $Ni_3HITP_2$, wherein $Ni_3BHT$ displays two well resolved peaks under negative polarization that indicate two unique chemical environments for $^7$Li sorption.

indicates two distinct ionic $^7$Li chemical environments with distinct nuclear quadrupole coupling interactions, albeit with similar isotropic chemical shifts due to lithium's small diamagnetic chemical shift range.[46] Overall, the shift to higher frequency and the emergence of a new $^7$Li chemical environment in $Ni_3BHT$ are in line with earlier reports of $Li^+$ intercalation into a carbon framework.[47] On the other hand, because $Ni_3HITP_2$ exhibits micropores and displays double-layer ion adsorption, its $^7$Li NMR spectrum displays a single Gaussian-like resonance (Figure 4B) for $Li^+$ adsorbed in its porous structure.

To further investigate the possibility of intercalation in $Ni_3BHT$, $^7$Li NMR spectra were acquired with cross-polarization magic angle spinning (CPMAS). Figure S11 compares spectra of the negatively polarized $Ni_3BHT$ sample obtained with a Bloch decay with that obtained with CPMAS, both obtained by coadding 1024 transients. Despite the theoretical enhancement of 2.6 to the peak intensity expected for $^1$H−$^7$Li cross-polarization, the spectrum acquired with a Bloch decay is much more intense. The peaks for that spectrum (red curve in


https://dx.doi.org/10.1021/jacs.0c10849
J. Am. Chem. Soc. XXXX, XXX, XXX−XXX

Figure S11) are also much broader, and the spinning sideband manifold extends much further, indicating that the CPMAS technique is selective for a particular Li-site. Considering that $^7$Li cross-polarization favors the excitation of lithium ions near $^1$H nuclei, this approach should restrict Li excitation to Li ions that are intercalated within $Ni_3BHT$ (~0 ppm) of the material while hindering the excitation of nonintercalated $Li^+$ (approximately −3 ppm) ions that are isolated from a proton-spin reservoir. To confirm these assignments, $^7Li\{^1H\}$ CPMAS was also performed on nonpolarized $Ni_3BHT$ and $Ni_3HITP_2$ samples. No observable CPMAS signal was detectable for nonpolarized $Ni_3BHT$ even using long contact times (5−8 ms), while nonpolarized $Ni_3HITP_2$ behaved similar to polarized $Ni_3HITP_2$, further supporting the assignments above. Figure S12 illustrates two-dimensional $^1H-^7Li$ heteronuclear correlation (HETCOR) spectra for the polarized $Ni_3BHT$ sample acquired with 100 and 500 $\mu$s contact times; these indicate a cross peak between the intercalated $Li^+$ sites and a broad $^1$H resonance from the organic components and sensitive to the contact time. (Figure S12b) A sharp $^1$H resonance (1 ppm) is assigned to MeCN, but no correlation to this resonance is observed within the HETCOR spectra (Figure S13). Although we cannot rule out the presence of trapped MeCN within the $Ni_3BHT$ sheets, the broad $^1$H resonance is consistent with partial desolvation of intercalated $Li^+$ ions.

X-ray absorption spectroscopy (XAS) indicated that the pseudocapacitive behavior of $Ni_3BHT$ is not Ni-based. The X-ray absorption near edge spectroscopy (XANES) at the Ni K edge revealed edge and pre-edge energies of 8.346 and 8.334 keV, respectively, for both pristine and polarized $Ni_3BHT$, indicating that the 2+ oxidation state of Ni persists during EC operation (Figure S14). Furthermore, analysis of the local coordination around Ni from the X-ray absorption fine structure (EXAFS) revealed essentially identical Ni coordination numbers of 4(±0.4) and 3.7(±0.4) before and after polarization (Figures S15 and S16 and Supporting Table 3). Likewise, the Ni−S bond length in $Ni_3BHT$ remains largely unchanged, although a slight decrease from 2.16 (±0.02) to 2.13 (±0.02) Å upon polarization suggests increased electron density on the S atoms. These observations suggest that redox processes are not metal based and instead center on the ligand. Indeed, high resolution X-ray photoelectron spectroscopy (XPS) shows that the C 1s and Ni 2p peaks are unaffected by polarization, and the only observable changes are with the S 2p peak (Figure S17). Specifically, deconvolution of the S signal into various chemical components with doublet structures of $2p_{1/2}$ and $2p_{3/2}$ reveals a loss of the S−H component and an appearance of the S−Li component upon polarization, indicating reduction and subsequent intercalation of $Li^+$ ions in close proximity to the electronegative S sites (Figure S18). Such a ligand-centered process has been noted in several studies of Ni-bis(dithiolene) complexes and is explained by the low energy of Ni d-orbitals compared to ligand-centered orbitals,[48] having also been invoked recently in a study employing $Cu_3BHT$ for Li-ion batteries.[49] Notably, the observed redox process differentiates $Ni_3BHT$ from other transition-metal-based pseudocapacitive materials wherein multiple oxidation states of the metal ions (Ru, Nb or Mo) are accessed during intercalation and are readily characterized by XAS studies.[9] Unfortunately, the extended conjugation structure over CPs makes it difficult to assign the exact changes in oxidation states of the ligands with any degree of certainty.

Nevertheless, the high specific capacitances and the large reductive potential window through intercalation-pseudocapacitance identify $Ni_3BHT$ as a promising negative electrode toward fabricating high-voltage asymmetric ECs.

The efficacy of $Ni_3BHT$ as a component in ECs was probed by constructing an asymmetric EC wherein $Ni_3BHT$ served as the negative electrode and activated carbon as the positive electrode (details in Supporting Information). CV and charge−discharge curves displayed respectively rectangular and triangular curves, while delivering high full-cell capacitances around 38 F/g in a 2.5 V voltage window (Figure 5A and Figure S19). Potential measurements of both the electrodes using an auxiliary Ag reference indicated that the cell operated within the stable voltage range of $Ni_3BHT$ while potentially allowing for even higher voltages (Figure 5B). Tests in a larger voltage window of 3 V displayed slightly distorted CVs at the terminal voltages, indicating the need for further optimization of charge balance between $Ni_3BHT$ and carbon electrodes (Figure S20).

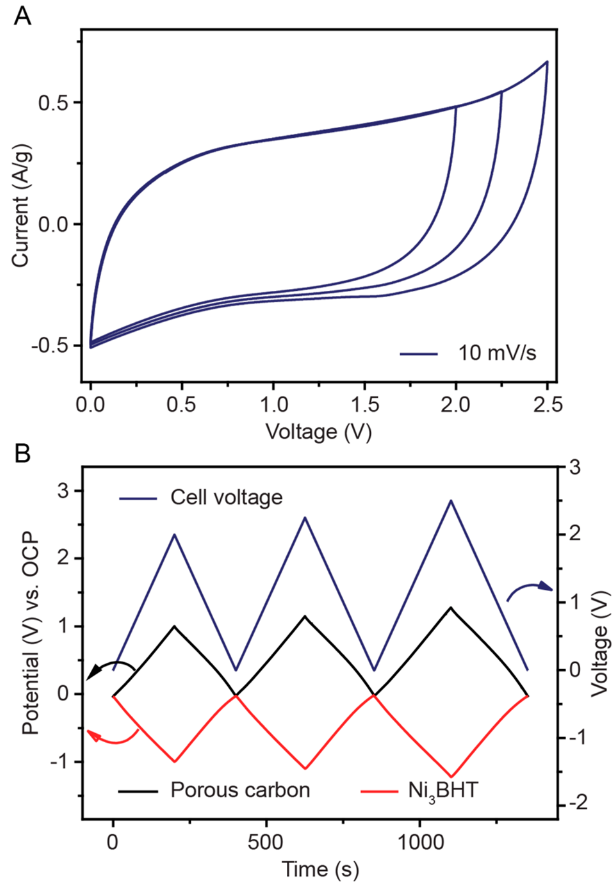


**Figure 5.** (A) CV curves of an asymmetric EC with $Ni_3BHT$ and porous carbon as the negative and positive electrodes, respectively. (B) Individual electrode potentials and full-cell potentials during cell operation from 0 to 2.5 V.

## CONCLUSIONS

The foregoing results show that nonporous CPs are excellent candidate materials for ECs despite their lack of porosity. As a first example in its class of nonporous CPs, $Ni_3BHT$ delivers a high specific capacitance of 245 F/g in a large reductive potential window of 1.7 V. Extensive electrochemical analyses revealed that a pseudocapacitive intercalation mechanism is responsible for the performance of $Ni_3BHT$. This is the first demonstration of a nonporous CP as an intercalative electrode material in ECs beyond inorganic materials. This work opens up 2D CPs as a new class of diverse and abundant materials that offer great chemical and structural tunability toward application in commercial ECs, complementing the utility of inorganic materials in this space.

## ■ ASSOCIATED CONTENT

### Supporting Information

The Supporting Information is available free of charge at https://pubs.acs.org/doi/10.1021/jacs.0c10849.

Synthetic details, instrumentation, and sample preparation for various spectroscopic techniques (PDF)

## ■ AUTHOR INFORMATION


### Corresponding Author

**Mircea Dincă** − *Department of Chemistry, Massachusetts Institute of Technology, Cambridge, Massachusetts 02138, United States;* orcid.org/0000-0002-1262-1264; Email: mdinca@mit.edu

### Authors

**Harish Banda** − *Department of Chemistry, Massachusetts Institute of Technology, Cambridge, Massachusetts 02138, United States;* orcid.org/0000-0002-1630-4450

**Jin-Hu Dou** − *Department of Chemistry, Massachusetts Institute of Technology, Cambridge, Massachusetts 02138, United States;* orcid.org/0000-0002-6920-9051

**Tianyang Chen** − *Department of Chemistry, Massachusetts Institute of Technology, Cambridge, Massachusetts 02138, United States;* orcid.org/0000-0003-3142-8176

**Nicole J. Libretto** − *Davidson School of Chemical Engineering, Purdue University, West Lafayette, Indiana 47907, United States*

**Madhusudan Chaudhary** − *Department of Chemistry, University of Alberta, Edmonton, Alberta T6G 2G2, Canada*

**Guy M. Bernard** − *Department of Chemistry, University of Alberta, Edmonton, Alberta T6G 2G2, Canada*

**Jeffrey T. Miller** − *Davidson School of Chemical Engineering, Purdue University, West Lafayette, Indiana 47907, United States;* orcid.org/0000-0002-6269-0620

**Vladimir K. Michaelis** − *Department of Chemistry, University of Alberta, Edmonton, Alberta T6G 2G2, Canada;* orcid.org/0000-0002-6708-7660

Complete contact information is available at: https://pubs.acs.org/10.1021/jacs.0c10849

### Author Contributions

[⊥]H.B and J.-H.D contributed equally.



### Funding

This work is supported by Automobili Lamborghini S.P.A. Part of the characterization was performed at the Centre for Nanoscale Systems (CNS), a member of the National Nanotechnology Infrastructure Network (NNIN), which is supported by the National Science Foundation under NSF Award No. 1541959. CNS is part of Harvard University.


### Notes

The authors declare no competing financial interest.

This work has been filed as part of U.S. Provisional Patent Application No. 62/908,297.

## ■ ACKNOWLEDGMENTS


J.-H.D. thanks Dr. Jian Li and Prof. Junliang Sun for help with the structural determination. H.B. thanks Dr. Michal A. Borysiewicz for support during initial setup of the project. V.K.M. acknowledges the Natural Sciences and Engineering Research Council (NSERC) of Canada, the Canadian Foundation for Innovation, Future Energy Systems and the Government of Alberta for research support.


## ■ REFERENCES


(1) Simon, P.; Gogotsi, Y. Materials for Electrochemical Capacitors. *Nat. Mater.* **2008**, *7* (11), 845−854.

(2) Salanne, M.; Rotenberg, B.; Naoi, K.; Kaneko, K.; Taberna, P.-L.; Grey, C. P.; Dunn, B.; Simon, P. Efficient Storage Mechanisms for Building Better Supercapacitors. *Nat. Energy* **2016**, *1* (6), 1−10.

(3) Choi, C.; Ashby, D. S.; Butts, D. M.; DeBlock, R. H.; Wei, Q.; Lau, J.; Dunn, B. Achieving High Energy Density and High Power Density with Pseudocapacitive Materials. *Nat. Rev. Mater.* **2020**, *5* (1), 5−19.

(4) Béguin, F.; Presser, V.; Balducci, A.; Frackowiak, E. Carbons and Electrolytes for Advanced Supercapacitors. *Adv. Mater.* **2014**, *26* (14), 2219−2251.

(5) Yang, X.; Cheng, C.; Wang, Y.; Qiu, L.; Li, D. Liquid-Mediated Dense Integration of Graphene Materials for Compact Capacitive Energy Storage. *Science* **2013**, *341* (6145), 534.

(6) Zhu, Y.; Murali, S.; Stoller, M. D.; Ganesh, K. J.; Cai, W.; Ferreira, P. J.; Pirkle, A.; Wallace, R. M.; Cychosz, K. A.; Thommes, M.; Su, D.; Stach, E. A.; Ruoff, R. S. Carbon-Based Supercapacitors Produced by Activation of Graphene. *Science* **2011**, *332* (6037), 1537−1541.

(7) Sun, L.; Campbell, M. G.; Dincă, M. Electrically Conductive Porous Metal−Organic Frameworks. *Angew. Chem., Int. Ed.* **2016**, *55* (11), 3566−3579.

(8) Xie, L. S.; Skorupskii, G.; Dincă, M. Electrically Conductive Metal−Organic Frameworks. *Chem. Rev.* **2020**, *120* (16), 8536−8580.

(9) Augustyn, V.; Simon, P.; Dunn, B. Pseudocapacitive Oxide Materials for High-Rate Electrochemical Energy Storage. *Energy Environ. Sci.* **2014**, *7* (5), 1597−1614.

(10) Simon, P.; Gogotsi, Y. Perspectives for Electrochemical Capacitors and Related Devices. *Nat. Mater.* **2020**, *19* (11), 1151−1163.

(11) Conway, B. E. Transition from "Supercapacitor" to "Battery" Behavior in Electrochemical Energy Storage. *J. Electrochem. Soc.* **1991**, *138* (6), 1539−1548.

(12) Brousse, T.; Bélanger, D.; Long, J. W. To Be or Not To Be Pseudocapacitive? *J. Electrochem. Soc.* **2015**, *162* (5), A5185−A5189.

(13) Simon, P.; Gogotsi, Y.; Dunn, B. Where Do Batteries End and Supercapacitors Begin? *Science* **2014**, *343* (6176), 1210−1211.

(14) Trasatti, S.; Buzzanca, G. Ruthenium Dioxide: A New Interesting Electrode Material. Solid State Structure and Electrochemical Behaviour. *J. Electroanal. Chem. Interfacial Electrochem.* **1971**, *29* (2), A1−A5.

(15) Kuo, S.-L.; Wu, N.-L. Investigation of Pseudocapacitive Charge-Storage Reaction of $MnO_2$ • $NH_2O$ Supercapacitors in Aqueous Electrolytes. *J. Electrochem. Soc.* **2006**, *153* (7), A1317−A1324.

(16) Lindström, H.; Södergren, S.; Solbrand, A.; Rensmo, H.; Hjelm, J.; Hagfeldt, A.; Lindquist, S.-E. $Li^+$ Ion Insertion in $TiO_2$ (Anatase). 2. Voltammetry on Nanoporous Films. *J. Phys. Chem. B* **1997**, *101* (39), 7717−7722.

(17) Augustyn, V.; Come, J.; Lowe, M. A.; Kim, J. W.; Taberna, P.-L.; Tolbert, S. H.; Abruña, H. D.; Simon, P.; Dunn, B. High-Rate Electrochemical Energy Storage through $Li^+$ Intercalation Pseudocapacitance. *Nat. Mater.* **2013**, *12* (6), 518−522.

(18) Sun, H.; Mei, L.; Liang, J.; Zhao, Z.; Lee, C.; Fei, H.; Ding, M.; Lau, J.; Li, M.; Wang, C.; Xu, X.; Hao, G.; Papandrea, B.; Shakir, I.; Dunn, B.; Huang, Y.; Duan, X. Three-Dimensional Holey-Graphene/Niobia Composite Architectures for Ultrahigh-Rate Energy Storage. *Science* **2017**, *356* (6338), 599.

(19) Wang, X.; Mathis, T. S.; Li, K.; Lin, Z.; Vlcek, L.; Torita, T.; Osti, N. C.; Hatter, C.; Urbankowski, P.; Sarycheva, A.; Tyagi, M.; Mamontov, E.; Simon, P.; Gogotsi, Y. Influences from Solvents on Charge Storage in Titanium Carbide MXenes. *Nat. Energy* **2019**, *4* (3), 241−248.

(20) Acerce, M.; Voiry, D.; Chhowalla, M. Metallic 1T Phase $MoS_2$ Nanosheets as Supercapacitor Electrode Materials. *Nat. Nanotechnol.* **2015**, *10* (4), 313−318.

(21) Lukatskaya, M. R.; Kota, S.; Lin, Z.; Zhao, M.-Q.; Shpigel, N.; Levi, M. D.; Halim, J.; Taberna, P.-L.; Barsoum, M. W.; Simon, P.; Gogotsi, Y. Ultra-High-Rate Pseudocapacitive Energy Storage in Two-Dimensional Transition Metal Carbides. *Nat. Energy* **2017**, *2* (8), 17105.

(22) Lukatskaya, M. R.; Mashtalir, O.; Ren, C. E.; Dall'Agnese, Y.; Rozier, P.; Taberna, P. L.; Naguib, M.; Simon, P.; Barsoum, M. W.; Gogotsi, Y. Cation Intercalation and High Volumetric Capacitance of Two-Dimensional Titanium Carbide. *Science* **2013**, *341* (6153), 1502−1505.

(23) Givaja, G.; Amo-Ochoa, P.; Gómez-García, C. J.; Zamora, F. Electrical Conductive Coordination Polymers. *Chem. Soc. Rev.* **2012**, *41* (1), 115−147.

(24) Huang, X.; Sheng, P.; Tu, Z.; Zhang, F.; Wang, J.; Geng, H.; Zou, Y.; Di, C.; Yi, Y.; Sun, Y.; Xu, W.; Zhu, D. A Two-Dimensional $\pi$−d Conjugated Coordination Polymer with Extremely High Electrical Conductivity and Ambipolar Transport Behaviour. *Nat. Commun.* **2015**, *6* (1), 1−8.

(25) Sheberla, D.; Sun, L.; Blood-Forsythe, M. A.; Er, S.; Wade, C. R.; Brozek, C. K.; Aspuru-Guzik, A.; Dincă, M. High Electrical Conductivity in $Ni_3$(2,3,6,7,10,11-Hexaiminotriphenylene)$_2$, a Semi-conducting Metal−Organic Graphene Analogue. *J. Am. Chem. Soc.* **2014**, *136* (25), 8859−8862.

(26) Dou, J.-H.; Sun, L.; Ge, Y.; Li, W.; Hendon, C. H.; Li, J.; Gul, S.; Yano, J.; Stach, E. A.; Dincă, M. Signature of Metallic Behavior in the Metal−Organic Frameworks $M_3$(Hexaiminobenzene)$_2$ (M = Ni, Cu). *J. Am. Chem. Soc.* **2017**, *139* (39), 13608−13611.

(27) Kambe, T.; Sakamoto, R.; Hoshiko, K.; Takada, K.; Miyachi, M.; Ryu, J.-H.; Sasaki, S.; Kim, J.; Nakazato, K.; Takata, M.; Nishihara, H. $\pi$-Conjugated Nickel Bis(Dithiolene) Complex Nano-sheet. *J. Am. Chem. Soc.* **2013**, *135* (7), 2462−2465.

(28) Furukawa, H.; Cordova, K. E.; O'Keeffe, M.; Yaghi, O. M. The Chemistry and Applications of Metal-Organic Frameworks. *Science* **2013**, *341* (6149), 1230444.

(29) Choi, K. M.; Jeong, H. M.; Park, J. H.; Zhang, Y.-B.; Kang, J. K.; Yaghi, O. M. Supercapacitors of Nanocrystalline Metal−Organic Frameworks. *ACS Nano* **2014**, *8* (7), 7451−7457.

(30) Sheberla, D.; Bachman, J. C.; Elias, J. S.; Sun, C.-J.; Shao-Horn, Y.; Dincă, M. Conductive MOF Electrodes for Stable Supercapacitors with High Areal Capacitance. *Nat. Mater.* **2017**, *16* (2), 220−224.

(31) Feng, D.; Lei, T.; Lukatskaya, M. R.; Park, J.; Huang, Z.; Lee, M.; Shaw, L.; Chen, S.; Yakovenko, A. A.; Kulkarni, A.; Xiao, J.; Fredrickson, K.; Tok, J. B.; Zou, X.; Cui, Y.; Bao, Z. Robust and Conductive Two-Dimensional Metal−organic Frameworks with Exceptionally High Volumetric and Areal Capacitance. *Nat. Energy* **2018**, *3* (1), 30−36.

(32) Li, W.-H.; Ding, K.; Tian, H.-R.; Yao, M.-S.; Nath, B.; Deng, W.-H.; Wang, Y.; Xu, G. Conductive Metal−Organic Framework Nanowire Array Electrodes for High-Performance Solid-State Super-capacitors. *Adv. Funct. Mater.* **2017**, *27* (27), 1702067.

(33) Amores, M.; Wada, K.; Sakaushi, K.; Nishihara, H. Reversible Energy Storage in Layered Copper-Based Coordination Polymers: Unveiling the Influence of the Ligand's Functional Group on Their Electrochemical Properties. *J. Phys. Chem. C* **2020**, *124* (17), 9215−9224.

(34) Bi, S.; Banda, H.; Chen, M.; Niu, L.; Chen, M.; Wu, T.; Wang, J.; Wang, R.; Feng, J.; Chen, T.; Dincă, M.; Kornyshev, A. A.; Feng, G. Molecular Understanding of Charge Storage and Charging Dynamics in Supercapacitors with MOF Electrodes and Ionic Liquid Electro-lytes. *Nat. Mater.* **2020**, *19* (5), 552−558.

(35) Meng, X.; Kolodzeiski, E.; Huang, X.; Timmer, A.; Schulze Lammers, B.; Gao, H.-Y.; Mönig, H.; Liu, L.; Xu, W.; Amirjalayer, S.; Zhu, D.; Fuchs, H. Tunable Thiolate Coordination Networks on Metal Surfaces. *ChemNanoMat* **2020**, *6* (10), 1479−1484.

(36) Sun, L.; Park, S. S.; Sheberla, D.; Dincă, M. Measuring and Reporting Electrical Conductivity in Metal−Organic Frameworks: $Cd_2$(TTFTB) as a Case Study. *J. Am. Chem. Soc.* **2016**, *138* (44), 14772−14782.

(37) Mathis, T. S.; Kurra, N.; Wang, X.; Pinto, D.; Simon, P.; Gogotsi, Y. Energy Storage Data Reporting in Perspective—Guidelines for Interpreting the Performance of Electrochemical Energy Storage Systems. *Adv. Energy Mater.* **2019**, *9* (39), 1902007.

(38) Segalini, J.; Iwama, E.; Taberna, P.-L.; Gogotsi, Y.; Simon, P. Steric Effects in Adsorption of Ions from Mixed Electrolytes into Microporous Carbon. *Electrochem. Commun.* **2012**, *15* (1), 63−65.

(39) Moitzheim, S.; De Gendt, S.; Vereecken, P. M. Investigation of the Li-Ion Insertion Mechanism for Amorphous and Anatase $TiO_2$ Thin-Films. *J. Electrochem. Soc.* **2019**, *166* (2), A1−A9.

(40) Chodankar, N. R.; Patil, S. J.; Rama Raju, G. S.; Lee, D. W.; Dubal, D. P.; Huh, Y. S.; Han, Y.-K. Two-Dimensional Materials for High-Energy Solid-State Asymmetric Pseudocapacitors with High Mass Loadings. *ChemSusChem* **2020**, *13* (6), 1582−1592.

(41) Banda, H.; Daffos, B.; Périé, S.; Chenavier, Y.; Dubois, L.; Aradilla, D.; Pouget, S.; Simon, P.; Crosnier, O.; Taberna, P.-L.; Duclairoir, F. Ion Sieving Effects in Chemically Tuned Pillared Graphene Materials for Electrochemical Capacitors. *Chem. Mater.* **2018**, *30* (9), 3040−3047.

(42) Banda, H.; Périé, S.; Daffos, B.; Taberna, P.-L.; Dubois, L.; Crosnier, O.; Simon, P.; Lee, D.; De Paëpe, G.; Duclairoir, F. Sparsely Pillared Graphene Materials for High-Performance Supercapacitors: Improving Ion Transport and Storage Capacity. *ACS Nano* **2019**, *13* (2), 1443−1453.

(43) Levi, M. D.; Levy, N.; Sigalov, S.; Salitra, G.; Aurbach, D.; Maier, J. Electrochemical Quartz Crystal Microbalance (EQCM) Studies of Ions and Solvents Insertion into Highly Porous Activated Carbons. *J. Am. Chem. Soc.* **2010**, *132* (38), 13220−13222.

(44) Eliad, L.; Salitra, G.; Soffer, A.; Aurbach, D. Ion Sieving Effects in the Electrical Double Layer of Porous Carbon Electrodes: Estimating Effective Ion Size in Electrolytic Solutions. *J. Phys. Chem. B* **2001**, *105* (29), 6880−6887.

(45) Li, Y.; Shao, H.; Lin, Z.; Lu, J.; Liu, L.; Duployer, B.; Persson, P. O. Å.; Eklund, P.; Hultman, L.; Li, M.; Chen, K.; Zha, X.-H.; Du, S.; Rozier, P.; Chai, Z.; Raymundo-Piñero, E.; Taberna, P.-L.; Simon, P.; Huang, Q. A General Lewis Acidic Etching Route for Preparing MXenes with Enhanced Electrochemical Performance in Non-Aqueous Electrolyte. *Nat. Mater.* **2020**, *19* (8), 894−899.

(46) Michaelis, V. K.; Levin, K.; Germanov, Y.; Lelong, G.; Kroeker, S. Ultrahigh-Resolution $^7$Li Magic-Angle Spinning Nuclear Magnetic Resonance Spectroscopy by Isotopic Dilution. *Chem. Mater.* **2018**, *30* (16), 5521−5526.

(47) Hayes, S. E.; Guidotti, R. A.; Even, W. R.; Hughes, P. J.; Eckert, H. $^7$Li Solid-State Nuclear Magnetic Resonance as a Probe of Lithium Species in Microporous Carbon Anodes. *J. Phys. Chem. A* **2003**, *107* (19), 3866−3876.

(48) Kusamoto, T.; Nishihara, H. Zero-, One- and Two-Dimen-sional Bis(Dithiolato)Metal Complexes with Unique Physical and Chemical Properties. *Coord. Chem. Rev.* **2019**, *380*, 419−439.

(49) Wu, Z.; Adekoya, D.; Huang, X.; Kiefel, M. J.; Xie, J.; Xu, W.; Zhang, Q.; Zhu, D.; Zhang, S. Highly Conductive Two-Dimensional (2D) Metal-Organic Framework (MOFs) for Resilient Lithium Storage with Superb Rate Capability. *ACS Nano* **2020**, *14*, 12016.



https://dx.doi.org/10.1021/jacs.0c10849
J. Am. Chem. Soc. XXXX, XXX, XXX−XXX